Optics Letters

Adaptive feedback-driven probabilistic shaping for high-order modulation formats in a fiber–THz seamless integration system at 320 GHz

Xiang Liu,[1,2] Jiao Zhang,[1,2,*] Min Zhu,[1,2] Junhao Zhang,[1] Weidong Tong,[1,2] Zhigang Xin,[1,2] Bingchang Hua,[2] Yuancheng Cai,[1,2] Mingzheng Lei,[2] Bo Liu,[3] and Jianjun Yu[2,4]

[1]National Mobile Communications Research Laboratory, Southeast University, Nanjing 210096, China
[2]Purple Mountain Laboratories, Nanjing, Jiangsu 211111, China
[3]Nanjing University of Information Science and Technology, Nanjing, Jiangsu 10044, China
[4]Fudan University, Shanghai, 220 Handan Road 200433, China
*jiaozhang@seu.edu.cn

Received 8 September 2023; revised 8 November 2023; accepted 10 November 2023; posted 13 November 2023; published 00 xxxxxx 0000

In this Letter, we propose a novel adaptive feedback-driven probabilistic constellation-shaping (FBD-PCS) method based on the robustness evaluation criteria and employ variational autoencoder (VAE)-based equalizers to implement polarization demultiplexing and nonlinear equalization for the recovery of high-order PCS-QAM signals. We experimentally demonstrate the fiber–THz 2 *times* 2 MIMO system with a net rate of 366.4 Gbit/s using dual-polarization 40 Gbaud PCS-64QAM signal over a 20 km SSMF and 6 m wireless link. Specifically, the feedback mechanism drives the fiber–THz system to solve optimization problems, adaptively matching the optimized distribution of transmitted symbols that maximizes normalized generalized mutual information (NGMI). We also examine six scenarios to explore nonlinear resistances of FBD-PCS symbols and the robustness of VAE-based equalizers. The results demonstrate the superiority of FBD-PCS over the Maxwell–Boltzmann (M–B) distributions in practical nonlinear-dominant systems. Additionally, the FBD-PCS signals can break limitations for ultrahigh rate transmission with the help of advanced equalizers.

https://doi.org/10.1364/OL.505468

Fiber–terahertz (THz, 300 GHz 10 THz) integrated system with the photonics-aided scheme is widely recognized as a promising technology for facilitating future 6G connectivity [1]. Commercial digital signal processing (DSP) algorithms in optical fiber communication can leverage fiber-wireless systems for ultrahigh rate transmissions [2]. Moreover, substantial advancements in signal generation, modulation, and detection have expedited the seamless integration of wired and wireless systems.

Probabilistic constellation shaping (PCS) is a well-established technique in fiber-wireless integrated systems that utilize symmetric Maxwell–Boltzmann (M–B) distribution to generate signals with enhanced nonlinear resistances [3]. Although the mutual information (MI) of M–QAM modulation can be maximized in approximate AWGN channels when signals follow M–B distributions, this approximation for the fiber–THz channel becomes inaccurate in cases where the nonlinearity is dominant [4]. End-to-end (E2E) learning has emerged as an intelligent approach to adaptively learn optimal probabilistic distributions for high-order M–QAM signal, jointly trained to match uncertain channels best [5]. However, a challenge of optimizing PCS is accurately estimating cost function gradients in terms of non-differentiable probability distributions [6]. A simple feedback-based approach based on error counting is reported in the optical fiber system [7]. Furthermore, variational autoencoder (VAE)-based equalizers' rapid convergence behavior is advantageous for the simulated time-varying channels [8,9], where the gradually converging constant modulus algorithm (CMA)-based equalizers perform significantly worse for the recovery of high-order PCS-QAM signals [10].

In this Letter, we propose an efficient E2E feedback-driven PCS (FBD-PCS) method based on the received error rate matrix (ERM), simultaneously considering the characteristics of time variability and instability in the fiber–THz system. This method is not restricted to the symmetric probability distributions and is compatible with any desired shaping entropy H. Furthermore, based on [8], we employ a modified probability-aware vector-quantized VAE (VQ-VAE) equalizer combined with a complex-valued 2 × 2 MIMO framework to implement polarization demultiplexing and nonlinear equalization for dual-polarized PCS-QAM signals in practical fiber–THz systems, which drags the equalizer output to stay close to the codebook by making use of variational inference theory. Additionally, we examine six scenarios to explore the effectiveness of the FBD-PCS symbols and the robustness of VAE-based equalizers for the fiber–THz integrated system. We successfully demonstrate the fiber–THz 2 × 2 MIMO transmission system with a line rate of 462.4 Gbit/s and a net rate of 366.4 Gbit/s using a dual-polarization 40 Gbaud FBD-PCS 64QAM over a 20 km standard single-mode fiber (SSMF) and 6 m wireless link without using the THz power amplifier.

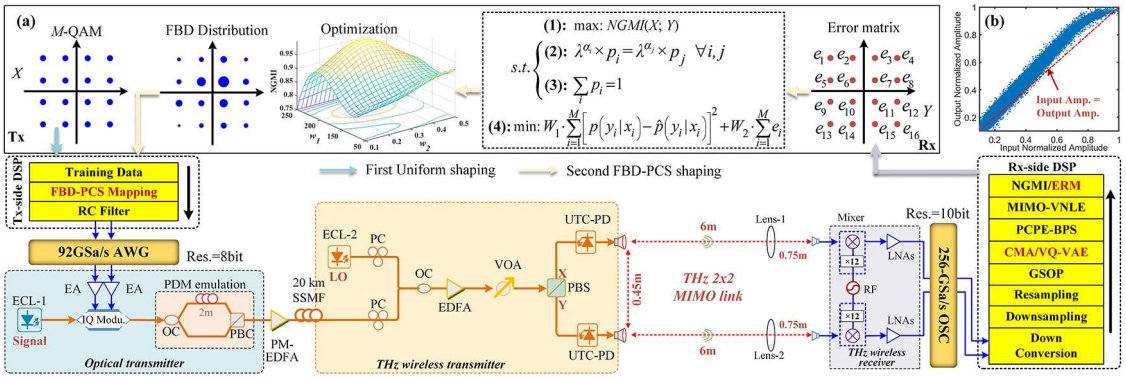

Fig. 1. Experimental setup of a dual-polarized fiber–THz 2 × 2 MIMO wireless transmission system including the offline DSP algorithm. (a) Principle of the FBD-PCS training method. (b) Normalized amplitude (AM/AM curves) response of the system.

A uniformly distributed sequence $x \in X$ is firstly transmitted from the transmitter to the receiver through the integrated fiber–THz system, where the received signals Y suffer different impairments. At the receiver side, the error number e_i at each point is counted to generate an error matrix $[e_1, \ldots, e_M]$, which is utilized to address the optimization problems, as depicted in Fig. 1(a). Figure 1(b) illustrates the typical nonlinear effect in the system. The detrimental nonlinear effect becomes more severe for signals with higher power. Equation (1) is subject to (*s.t.*) Eqs. (2) and (3), which aims to obtain optimal shaping probability vector $[p_1, \ldots, p_M]$ that maximizes normalized generalized MI (NGMI), i.e., *NGMI(X; Y)* instead of BER in [7]. Equation (2) specifies that if one of the two selected constellations (C_i and C_j) has experienced a high error rate value α, it should have a lower probability of being selected. p_i and p_j respresent the corresponding probabilities of the symbol. The ERM value $[\alpha_1, \ldots, \alpha_M]$ is normalized by dividing each error number e_i by the maximum number e_{MAX}, i.e., $\alpha_i = e_i/e_{MAX}$. The hyperparameter λ can be adjusted to control information entropy, $H(X, p_i)$. Equation (3) guarantees that the total of probabilities assigned to all symbols is 1. We further propose an efficient evaluation criterion in the time-varying system, as presented in Eq. (4). The approximate conditional probability $\hat{p}(y|x)$ and true conditional probability $p(y|x)$ can be estimated. The first term in Eq. (4), the expected likelihood, which explains the robustness of channel state information between the uniform symbols and feedback shaping symbols. The second term in Eq. (4) guarantees a minimum error number. W_1 and W_2 are introduced to maintain the order of magnitude agreement. By solving optimization problems with Eq. (4)–(4), optimizing weights W_1 and W_2, maximum *NGMI(X; Y)* can be achieved. An optimized FBD is obtained, and the constant composition distribution matching (CCDM) technique is employed to implement symbol shaping. And then FBD-PCS shaping symbols are subsequently sent to the fiber–THz system.

The experimental setup of our fiber–THz 2 × 2 MIMO system at 320 GHz is shown in Fig. 1. The electrical baseband signal is generated from a 92 Gsa/s arbitrary waveform generator (AWG) with 3 dB analog bandwidth of 32 GHz and 8-bit resolution. The signal is then amplified by two 40 GHz electrical amplifiers (EAs) before driving a 35 GHz I/Q modulator. The optical signal is amplified by a polarization-maintaining erbium-doped fiber amplifier (PM-EDFA). The optical signal and the ECL-2 operating at 193.3 THz as a local oscillator (LO) are coupled and transmitted over a 20 km SSMF. The

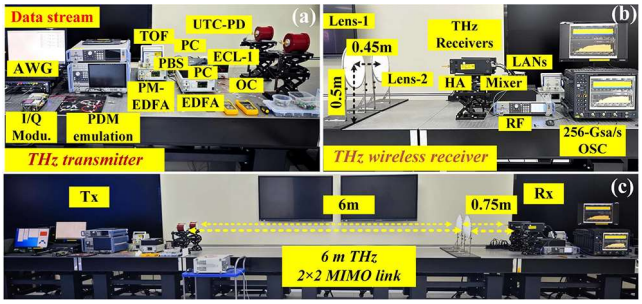

Fig. 2. Photos of (a) THz transmitter side. (b) THz wireless receiver side. (c) 6 m THz 2 × 2 MIMO transmission link.

coupled signals are amplified using an EDFA to drive commercial unitravelling-carrier photodiode (UTC-PD) effectively to enhance signal strength. A variable optical attenuator (VOA) is employed to adjust the input optical power into UTC-PD. A polarization beam splitter (PBS) is employed to split the combined lightwaves into two polarizations, which are then upconverted to THz-wave wireless signals. The polarization controllers (PCs) are used to adjust the incident polarization state to maximize optical power into polarization-sensitive UTC-PDs and balance the optical power of two polarization components.

Two parallel THz signals generated from the UTC-PDs are transmitted over the 6 m 2 × 2 MIMO wireless link. Two lenses (Lens-1 and Lens-2) are employed to maximize the signal power at the receiver, which can facilitate the THz-wave high-accuracy alignment to the horn antenna (HA). The lateral separation between the two parallel wireless links is 0.45 m. The THz transmitter and receiver are positioned at a height of 0.5 m to mitigate the effects of multi-path fading resulting from the ground reflections, and there is a distance of 0.75 m between the lens and the THz receiver. The THz-wave signals are received using two parallel HAs equipped with WR-2.2 waveguide interfaces, providing a gain of 26 dBi. Electronic LO sources drive THz receivers to implement analog downconversion, and each has a mixer and a × 12 frequency multiplier. The obtained intermediate-frequency (IF) signal at 23 GHz is then boosted by a pair of electrical low-noise amplifiers (LNAs) and captured by a 256 Gsa/s digital storage oscilloscope (OSC) for offline processing. Figure 2 gives the corresponding photos of the experimental setup.

The block diagram of offline DSP is also depicted in Fig. 1. The number of transmitted symbols is 262144 (2^{18}). We can

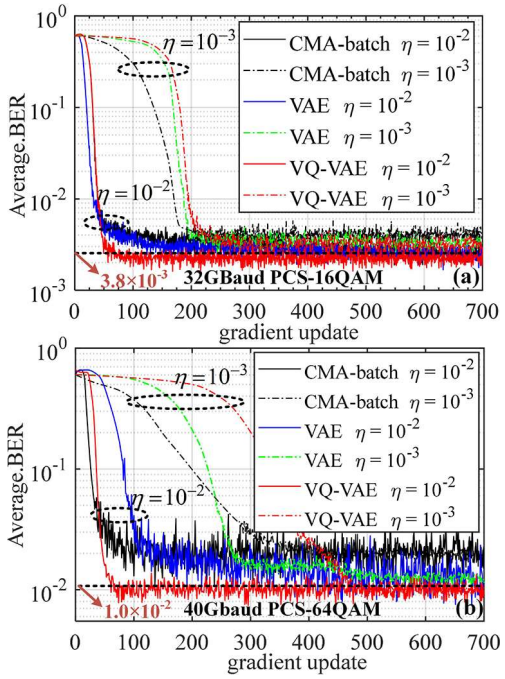

Fig. 3. Convergence behavior of three equalizers with different learning rates for (a) PCS-16QAM and (b) PCS-64QAM.

obtain the target entropy by tuning hyperparameter value λ, and the ERM value is calculated according to the decision criterion. At the Tx-side offline DSP, a raised-cosine (RC) filter with a roll-off factor of 0.01 is deployed. At the Rx-side offline DSP, the captured signals are downconverted and then resampled to two samples per symbol, the squaring time recovery, the polarization demultiplexing and nonlinear equalization based on the proposed VQ-VAE equalizer with a complex-valued MIMO model, and the frequency offset estimation (FOE). For the phase noise estimation, we employ a flexible and robust algorithm comprising principal component-based phase estimation (PCPE) and blind phase search (BPS). A second-order 189-tap Volterra nonlinear equalizer with MIMO (MIMO-VNLE) compensates for I/Q imbalance, linear, and nonlinear impairments. Finally, NGMI and ERM values can be calculated.

We first investigate convergence behaviors of the VAE-based and CMA-batch equalizers. We implement the CMA-batch equalizer using a batch-wise updating scheme, for which the constant modulus criterion is used as the cost function for training. For all equalizers under investigation, we consider a 40 Gbaud PCS-64QAM transmission at the input power into UTC-PD is 11.5 dBm, and the learning rate is η = 0.01, 0.001. Figure 3 shows the average BER evolution of different equalizers as increasing the number of performed gradient updates. For the considered configurations, we observe that (i) there exists an optimal value that trades off the system performance against the convergence speed and computational complexity. (ii) The CMA-batch and VAE equalizers suffer from training instability, especially for the relatively large learning rate η = 0.01. (iii) The VQ-VAE equalizer is more efficient and robust to variations in modulation orders and learning rates compared with the CMA-batch equalizer and conventional VAE equalizer, which is advantageous for time-varying and nonlinear channels.

We further examine nonlinear resistances of the proposed FBD-PCS method by introducing six different configurations at 11.5 dBm input power, considering different modulation orders and transmission rates, as shown in Fig. 4. From the considered scenarios, we make the following observations: (i) in each scenario, it is a well-established fact that the received symbols in the outer region are more susceptible to nonlinear impairments, particularly during high-speed and high-order signal transmission. (ii) During the high-speed signal transmission in scenarios 2, 4, and 5, constellation points received at the outermost positions experience saturation and distortion when using uniform shaping signals, resulting in high ERM values at the corners caused by limited bandwidth and nonlinear distortions. (iii) During the high-order signal transmission in scenarios 3–6, the constellation points with high ERM value suffer from nonlinear distortions, especially for the outermost points, mainly due to the nonlinear channel and imperfect optoelectronic devices. However, by utilizing FBD-PCS shaping signals, the constellation point exhibiting high ERM value is assigned a low probability, particularly at the outermost points of the nonlinear system, resulting in an optimized constellation and effectively improving the nonlinear resistances of the system. The obtained FBD-PCS distribution is valid for the true environment with dominant nonlinearity.

Next, Fig. 5 illustrates the NGMI improvements achieved by the FBD-PCS method compared with uniform and M–B shaping symbols, combined with the same configuration of the VQ-VAE equalizers. Since scenario 6 cannot reach the 0.83-NGMI threshold, we mainly analyze the performances of scenarios 1–4. For a fair comparison, the entropy value H of M–B is set the same

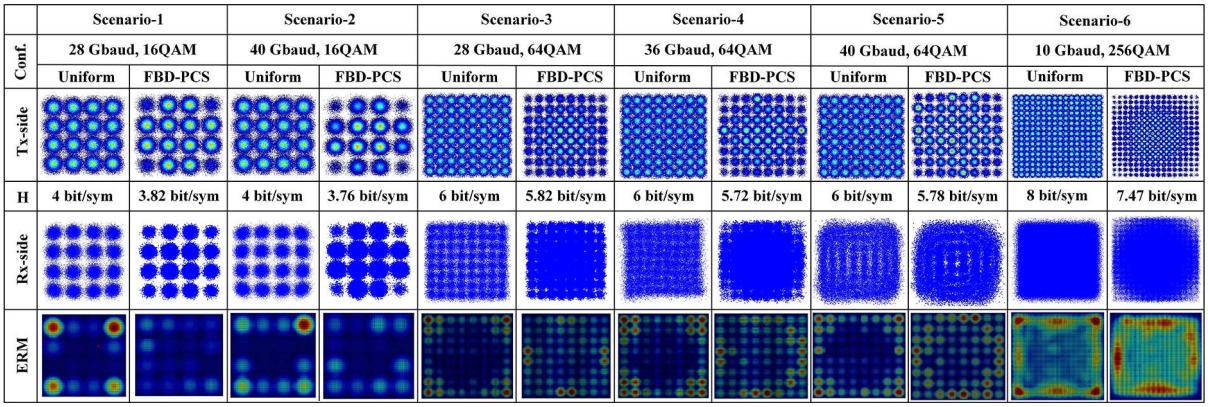

Fig. 4. Experimental results of the ERM value with and without FBD-PCS in six scenarios at 11.5 dBm input power into UTC-PD. Increased brightness corresponds to a higher ERM value, representing the magnitude of the error rate.

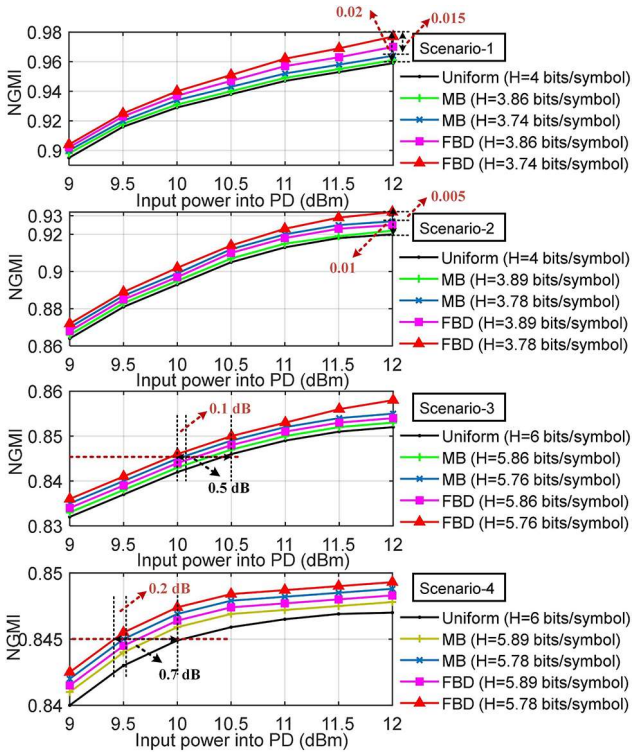

Fig. 5. Experimental results for the NGMI performance comparison of FBD-PCS with uniform and MB distributions.

as FBD-PCS in all four scenarios. From the results in Fig. 5, we can conclude that (i) uniform signal has a lower NGMI performance than the PCS signal because the outermost points are the dominant sources of symbol errors. (ii) While the M–B shaping signals show acceptable performance, the NGMI of FBD-PCS is either comparable or superior to the M–B distributions when the entropy value H is the same and achieves 0.015 and 0.005 gain in scenarios 1 and 2. (iii) In scenarios 3 and 4 for high-order signals, the NGMI value tends to be a saturation value even if the input power increases due to nonlinear limitations. The superiority of the proposed FBD method achieves 0.1 dB and 0.2 dB gains in receiver sensitivity compared with M–B shaping signals at the 0.845-NGMI threshold.

Finally, Fig. 6 depicts the NGMI performance versus baud rates for the received PCS-64QAM signals over a 20 km SSMF and 6 m wireless delivery at 12 dBm input power into the UTC-PD and the same entropy is 5.78. Considering the 0.83-NGMI threshold with error-free decoding, the highest baud rate for the FBD-64QAM signals transmission we can achieve is 40 Gbaud, while the PCS-64QAM with M–B signals cannot reach the 0.83-NGMI threshold. Therefore, by employing dual-polarized FED-PCS 64QAM signals and the VQ-VAE nonlinear equalizer, we can break the nonlinear limitation at 40 Gbaud and achieve a line rate of 462.4 Gbit/s ($5.78 \times 40 \times 2 = 462.4$ Gbit/s) at the 0.83-NGMI threshold. Considering the SD-FEC with a 25% overhead, the net data rate is 366.4 Gbit/s ($[5.78 \times 6 \times (1–0.8)] \times 40 \times 2 = 366.4$ Gbit/s). Note that, this work does not

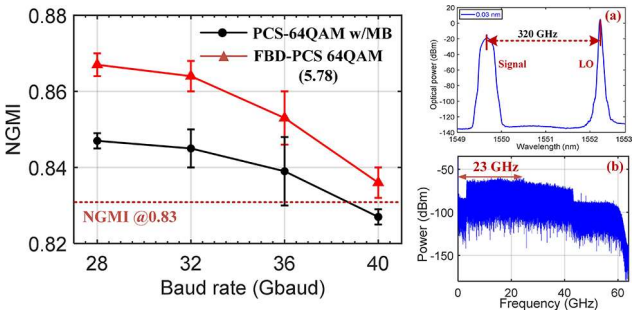

Fig. 6. NGMI versus baud rate for MB-PCS and FBD-PCS 64QAM over a 20 km SSMF and 6 m THz wireless link.

consider code modulation compatible with asymmetric shaping. Figure 6(a) shows the spectrum after coupling with a resolution of 0.03 nm. Figure 6(b) gives the electrical spectrum of IF signals.

In conclusion, we present a novel adaptive FBD-PCS method and demonstrate a dual-polarized fiber–THz 2×2 MIMO system with a line rate of 462.4 Gbit/s using 40 Gbaud PCS-64QAM modulation over a 20 km SSMF and 6 m wireless link. Advanced nonlinear algorithms for high-order PCS-QAM signals can break through nonlinear limitations, facilitating ultrahigh data rate transmission. The proposed FBD-PCS method with the VQ-VAE nonlinear equalizers, relying on a low-complexity FBD training model, can be used to evaluate the complex channels and design constellation-shaping modulation for emerging services.

Funding. National Natural Science Foundation of China (62101121, 62101126, 62201393, 62201397, 62271135); Graduate Research and Innovation Projects of Jiangsu Province (SJCX21_0036).

Disclosures. The authors declare no conflicts of interest.

Data availability. Data underlying the results presented in this paper are not publicly available at this time but may be obtained from the authors upon reasonable request.

REFERENCES

1. M. Zhu, J. Zhang, B. Hua, *et al.*, Sci. China Inf. Sci. **66**, 113301 (2023).
2. J. Zhang, M. Zhu, M. Lei, *et al.*, Opt. Lett. **47**, 1214 (2022).
3. X. Li, J. Yu, L. Zhao, *et al.*, *Optical Fiber Communication Conference (OFC)* (2019), paper M4F.4.
4. F. R. Kschischang and S. Pasupathy, IEEE Trans. Inf. Theory **39**, 913 (1993).
5. T. O'shea and J. Hoydis, IEEE Trans. Cogn. Commun. Netw. **3**, 563 (2017).
6. F. A. Aoudia and J. Hoydis, in *IEEE Global Communications Conference* (2020), pp. 1–6.
7. A. Fallahpour, F. Alishahi, A. Minoofar, *et al.*, *Optical Fiber Communication Conference (OFC)* (2020), paper. M1G.3.
8. X. Liu, J. Zhang, M. Zhu, *et al.*, *European Conference on Optical Communication (ECOC)* (2023), paper. We.B.7.4.
9. J. Song, V. Lauinger, Y. Wu, *et al.*, "Blind channel equalization using vector-quantized 306 variational autoencoders," arXiv, arXiv:2302.11687 (2023).
10. J. Ding, M. Wang, W. Li, *et al.*, Opt. Lett. **47**, 3904 (2022).